Eur. Phys. J. E (2024) 47:12
https://doi.org/10.1140/epje/s10189-023-00400-9

THE EUROPEAN PHYSICAL JOURNAL E

Regular Article - Soft Matter

Dynamic structure factor of undulating vesicles: finite-size and spherical geometry effects with application to neutron spin echo experiments

Rony Granek[1,a], Ingo Hoffmann[2,b], Elizabeth G. Kelley[3,c], Michihiro Nagao[3,4,5], Petia M. Vlahovska[6], and Anton Zilman[7]

[1] Avram and Stella Goldstein-Goren Department of Biotechnology Engineering, and Ilse Katz Institute for Nanoscale Science and Technology, Ben-Gurion University of the Negev, 84105 Beer Sheva, Israel
[2] Institut Laue-Langevin (ILL), 71 Avenue des Martys, 38042 Grenoble, CEDEX 9, France
[3] Center for Neutron Research, National Institute of Standards and Technology, 100 Bureau Drive, Gaithersburg, MD 20899, USA
[4] Department of Materials Science and Engineering, University of Maryland, College Park, MD 20742, USA
[5] Department of Physics and Astronomy, University of Delaware, Newark, DE 19716, USA
[6] Department of Engineering Sciences and Applied Mathematics, Northwestern University, Evanston, IL 60208, USA
[7] Department of Physics, University of Toronto, 60 St George St, Toronto, ON M5S 1A7, Canada

Received 20 October 2023 / Accepted 11 December 2023 / Published online 14 February 2024

Abstract We consider the dynamic structure factor (DSF) of quasi-spherical vesicles and present a generalization of an expression that was originally formulated by Zilman and Granek (ZG) for scattering from isotropically oriented quasi-flat membrane plaquettes. The expression is obtained in the form of a multi-dimensional integral over the undulating membrane surface. The new expression reduces to the original stretched exponential form in the limit of sufficiently large vesicles, i.e., in the micron range or larger. For much smaller unilamellar vesicles, deviations from the asymptotic, stretched exponential equation are noticeable even if one assumes that the Seifert-Langer leaflet density mode is completely relaxed and membrane viscosity is neglected. To avoid the need for an exhaustive numerical integration while fitting to neutron spin echo (NSE) data, we provide a useful approximation for polydisperse systems that tests well against the numerical integration of the complete expression. To validate the new expression, we performed NSE experiments on variable-size vesicles made of a POPC/POPS lipid mixture and demonstrate an advantage over the original stretched exponential form or other manipulations of the original ZG expression that have been deployed over the years to fit the NSE data. In particular, values of the membrane bending rigidity extracted from the NSE data using the new approximations were insensitive to the vesicle radii and scattering wavenumber and compared very well with expected values of the effective bending modulus ($\tilde{\kappa}$) calculated from results in the literature. Moreover, the *generalized scattering theory* presented here for an undulating quasi-spherical shell can be easily extended to other models for the membrane undulation dynamics beyond the Helfrich Hamiltonian and thereby provides the foundation for the study of the nanoscale dynamics in more complex and biologically relevant model membrane systems.

1 Introduction

There has been growing interest in using dynamic scattering techniques to study the thermal undulations of soft membranes formed by surfactants, lipids, and polymers. Such techniques are an important complement to other characterization methods that measure the time-averaged amplitude of the undulations to determine the membrane elastic properties, such as the bending modulus, κ. Measuring the relaxation dynamics in the time domain provides insights into not only the membrane rigidity, but also the dominant dissipation mechanisms. In addition to being a more rigorous test

This article is dedicated to Fyl Pincus whose pioneering achievements, inspiring approach, and revolutionary ideas in soft condensed matter and biological physics have had a great impact on the entire community in general, and especially on the present authors, including on RG, EGK, MN, and AZ.

[a] e-mail: rgranek@bgu.ac.il (corresponding author)
[b] e-mail: hoffmann@ill.fr (corresponding author)
[c] e-mail: egk@nist.gov (corresponding author)

of theoretical models for equilibrium bending fluctuations, understanding the dissipation mechanisms provides information on material properties that also influence the timescale of nonequilibrium membrane shape changes from droplet fusion in microemulsions to curvature generation by proteins in biological membranes.

Various dynamic scattering techniques have been used to study membrane fluctuation dynamics including dynamic light scattering (DLS) [1,2], x-ray photon correlation spectroscopy (XPCS) [3,4], and neutron spin echo (NSE) [5–7]. Detection of single membrane/interface thermal undulations requires at least $q\xi \gg 1$, where ξ is a typical object size or structure correlation length ("cell size"), and q is the scattering wavenumber. The latter is determined by the wavelength of the incident beam, λ (assumed to be identical to that of the scattered beam), and the angle, Θ, between the scattered and incident beams. Recall that $\vec{q} = \vec{Q}_f - \vec{Q}_{in}$, where $\vec{Q}_f$ and $\vec{Q}_{in}$ are the scattered and incident beam wavevectors, such that $q = 2Q\sin(\Theta/2)$ with $Q_f = Q_{in} = Q = 2\pi/\lambda$, leading to $q = 4\pi\sin(\Theta/2)/\lambda$. Thus, for example, DLS is only able to detect thermal undulations of quasi-spherical vesicles or droplets of radius R (or "cell size" ξ) $\gtrsim 1\mu$m, and at times $\gtrsim 10\mu$s [1,2,8,9]. It is therefore not surprising that NSE has been the most useful technique to study liposomes, surfactant vesicles, and microemulsion droplets (as well as lamellar and bicontinuous phases) of size 20 nm $\lesssim R$, $\xi \lesssim 200$ nm and times 0.5 ns $\lesssim t \lesssim 50$ ns.

Two theoretical approaches have been primarily used to analyze NSE data from such systems, one by Milner and Safran [10] and the other by Zilman and Granek [11,12]. Milner and Safran explicitly considered the spherical geometry of vesicles and microemulsion droplets by applying the continuum thin spherical shell formalism of Lovesey and Schofield [13], for which they implicitly assumed that density fluctuations are proportional to the undulation amplitude. The dynamic structure factor[1] (DSF) is then expressed as a weighted sum of the (spherical harmonic) mode amplitude autocorrelation functions. Zilman and Granek (ZG) instead considered quasi-flat membrane plaquettes of size ξ, for which they assumed $q\xi \gg 1$ such that the actual large-scale geometry of the object of size ξ, e.g., the radius R of a sphere or the linear size of a flat membrane plaquette, would not matter. By accounting for the nonlinear relation between local-temporal density, expressed as a sum over all molecules placed at position $\vec{r}$, $\sum_i \delta(\vec{r} - \vec{r}_i(t))$, and the local-temporal undulation amplitude, they obtained an exponential dependence of the DSF on the (time-dependent) undulation amplitude mean square displacement (MSD). In addition, ZG analyzed explicitly the short-time relaxation asymptotic, where the MSD is $\sim t^{2/3}$, and obtained the DSF in the form of a stretched exponential decay,

$$S(q,t) \approx S(q)\exp\left[-(\Gamma_q t)^{\alpha}\right], \tag{1}$$

with a stretching exponent $\alpha = 2/3$, and a relaxation rate

$$\Gamma_q = \left(\frac{\Gamma[1/3]}{4\pi 4^{2/3}}\right)^{3/2}\frac{(k_BT)^{3/2}}{\eta\kappa^{1/2}}q^3. \tag{2}$$

The power-law behavior of the MSD at short times, $\sim t^{2/3}$, is consistent with the scaling assumption $\langle\Delta h^2(t)\rangle = \langle h^2\rangle\Phi(t/\tau_r)$ where $\Phi(x)$ is the scaling function, $\tau_r \approx \eta R^3/\kappa$ (setting $\xi \simeq R$) is the longest undulation relaxation time, and $\langle h^2\rangle \approx (k_BT/\kappa)R^2$ is the mean membrane roughness, in which we demand that the (dimensioned) MSD is independent of R for $t \ll \tau_r$, implying $\Phi(x) \sim x^{2/3}$ for $x \ll 1$ and leading to

$$\langle\Delta h^2(t)\rangle \approx \frac{k_BT}{\eta^{2/3}\kappa^{1/3}}t^{2/3}. \tag{3}$$

The convergence of the DSF to the asymptotic ZG result in quasi-spherical vesicles of radius R requires the following conditions: (i) large vesicles such that $\pi R \gg \delta$ where δ is the bilayer thickness, which allows access to enough undulation modes; (ii) access to a time range of $\tau_0 \ll t \ll \tau_r$ where τ_0 and τ_r are the shortest and longest undulation relaxation times, which is required to approach the $\sim t^{2/3}$ MSD asymptote; (iii) $q\sqrt{\langle h^2\rangle} \gg 1$, which is required for the stretched exponential to dominate the observed DSF relaxation. The latter condition, replacing $qR \gg 1$, requires larger wavenumbers that depend on the value of κ. These conditions are consistent with the scaling assumption $\Gamma_q = \frac{k_BT}{\eta R}q^2\Psi(q\bar{h})$ where $\Psi(x)$ is a scaling function and $\bar{h} \equiv \sqrt{\langle h^2\rangle} \approx \sqrt{k_BT/\kappa}\,R$. By demanding that Γ_q is independent of R for $q\bar{h} \gg 1$, which implies $\Psi(x) \sim x$ for $x \gg 1$, we obtain the scaling dependence in Eq. (2).

The time range $\tau_0 \ll t \ll \tau_r$ required to reach the asymptotic result is roughly fulfilled, even for the small vesicle sizes studied in NSE, albeit with some numerical errors. However, the q range measured in NSE often implies $q\bar{h} \lesssim 1$. Thus, finite-size effects due to the spherical membrane geometry become important and one may expect significant deviations from the asymptotic limit in the dominant relaxation regime probed with NSE. Indeed, the stretched exponential expression has been shown to fail to describe NSE data from small vesicles, especially when the center of mass diffusion of the vesicles is considered [17,18]. As a result, different fitting approaches have been developed to account for these finite-size effects in NSE data over the past two decades. For bicontinuous microemulsions, where the mean curvature is small, Monkenbusch and coworkers have used the integral ZG expressions with the large-scale cutoff ξ to numerically fit the DSF [19]. For small quasi-spherical vesicles, a non-relaxing fitted amplitude

[1] Following the theoretical soft-matter literature [8,10–12,14–16], the term "dynamic structure factor" is used here instead of the common equivalent experimental term "intermediate scattering function", even though in the experimental community, DSF typically refers to the energy domain.

was often added to account for the approach to saturation of the MSD, and therefore the DSF, at times $t \sim \tau_r$ [17]. While the latter can be justified qualitatively, it has no quantitative theoretical justification [17]. Moreover, it remains unclear how the actual finite-size spherical geometry effects come into play. For example, the spherical geometry gives rise to Bragg oscillations in the static structure factor[2] (SSF) with dips occurring at $qR = n\pi$ (n is an integer), and maxima for $qR = (n + 1/2)\pi$ whose envelope decays as $\sim q^{-2}$. However, in experimentally measured SSFs, such as measured by small angle neutron scattering (SANS), these dips are usually smeared out to a large extent by polydispersity in the vesicle radii, instrument resolution, and incoherence effects, and the corresponding effects on the DSF are not clear.

It is even more timely to reconsider NSE data analysis as recent advances in NSE instrumentation and developments in the theories can provide new insights into the membrane fluctuation dynamics. When Milner and Safran and Zilman and Granek developed their original data analysis frameworks, the maximum time accessible on NSE instruments was on the order of 10 ns to 40 ns. Current NSE spectrometers routinely measure timescales on the order of 100 ns and upwards of 1000 ns [20–22]. With this order of magnitude gain in accessible times, it is worthwhile to revisit the theoretical assumptions of the data analysis approaches.

At the same time, there have been several extensions to the Helfrich bending Hamiltonian used to describe the membrane undulation dynamics since it was first published 50 years ago [23]. The Helfrich model was extended by Seifert, Lipowsky, and coworkers to account for the area difference between the two leaflets composing the bilayer, and the associated expressions for the undulation dynamics were developed by Seifert and Langer [24–26], giving rise to two modes: one is a monolayer-leaflet compression-dilation mode, and the other is an undulation amplitude mode. The effect of these generalized dynamics on the DSF was studied by Watson and Brown [8,9,16]. Importantly, Watson and Brown showed that an initial compression-dilation modulation, that is generated by an oscillatory undulation, usually relaxes on a time scale much longer than the longest NSE time scale. This implies that the undulation amplitude is relaxing, on the NSE times-scale, with an "unrelaxed" (or "non-equilibrated"), effective, bending constant given by

$$\tilde{\kappa} = \kappa + 2K_m d^2 \tag{4}$$

where K_m is a monolayer compression modulus and d is the height of the neutral surface, but otherwise with no change to the form of relaxation and to the resulting MSD and DSF [8,9,16]. Alternatively, work by Hellweg and colleagues considered contributions from both the undulation and compression-dilation modes predicted by Seifert and Langer in their NSE data analysis [27].

A more recent extension focused on the contribution of the membrane shear viscosity to the energy dissipation of relaxing undulations in spherical vesicles, which was confirmed by Faizi et al. by flickering spectroscopy of giant unilamellar vesicles [28]. Other extensions to the Helfrich model have considered membrane thickness fluctuations [29–32], as well as the effects of solvent permeability through pores [33], embedding the membrane in a viscoelastic continuous fluid [34] or embedding a membrane in a structured (viscoelastic) fluid on the undulation dynamics [35]. It is quite possible that other extensions, such as theories that account for the structure of the membrane and surrounding fluids, are forthcoming.

Hence, it is highly desirable to formulate a *general scattering theory* for an undulating quasi-spherical "shell", as an alternative to that developed by Milner and Safran, that will be able to account for the finite-size spherical geometry of the membrane/interface applicable to both small unilamellar vesicles (SUVs) and large unilamellar vesicles (LUVs). Here, we shall derive a general expression for a quasi-spherical vesicle (in the form of a multi-dimensional integral) based on the very reasonable assumption that the undulations are described by stochastic deformation "field" $u(\Omega, t)$ that obeys Gaussian statistics (associated with a harmonic-type Hamiltonian) for which, in principle, all spatiotemporal correlation functions can be calculated. This general expression was derived by Zilman and Granek about 25 years ago but remained unpublished. Given the complexity of the general expression that limits significantly its numerical evaluation and practical use, here we take advantage of vesicle size polydispersity, to greatly simplify the expression with only a minor compromise in the overall accuracy. Moreover, our use of the approximation here is limited to the Helfrich Hamiltonian, and to undulation dynamics that are governed solely by the solvent-mediated Oseen hydrodynamic interaction. In doing so, we do not imply, however, that this is the accurate description of the undulation dynamics in small unilamellar vesicles at nanosecond timescales, and we compare the values of the bending modulus extracted from the NSE data to models for extra sources of dissipation that have been predicted to come into play at the nanosecond timescales.

2 Theory: dynamic structure factor of undulating vesicles

2.1 Review of spherical harmonics expansion of vesicle thermal undulations—statics and dynamics

For clarity, we summarize here well-known results for quasi-spherical vesicles. Consider a mono-disperse solution of non-interacting quasi-spherical vesicles. The

[2] The term vesicle "static structure factor" used here is equivalent to the term vesicle "form factor" commonly used in the small angle scattering community.

coordinate of a "point" (small membrane segment) on a weakly deformed vesicle can be represented as [10,36,37]

$$\vec{r}_s(\Omega,t) = R\hat{r}\,[1+u(\Omega,t)] \tag{5}$$

where $\hat{r}$ is the radial unit vector, $R = (3V/4\pi)^{1/3}$ is the radius of an equivalent sphere with volume V, and $\Omega = (\theta,\phi)$ is the 3D angle.

The deviation from the spherical shape, $u(\Omega,t)$, can be expanded in spherical harmonics $Y_{\ell m}(\Omega)$,

$$u(\Omega,t) = \sum_{\ell=2}^{\ell_{\max}} \sum_{m=-\ell}^{\ell} u_{\ell m}(t) Y_{\ell m}(\Omega) \tag{6}$$

where ℓ_{max} is the maximum number of physically realizable modes and is determined by the vesicle size,

$$\ell_{max} \simeq \pi R/\delta \tag{7}$$

where δ is the bilayer thickness. Recall that the spherical harmonics can be expressed as

$$Y_{\ell m} = n_{\ell m} P_{\ell m}(\cos\theta) e^{im\phi}, \quad n_{\ell m} = \sqrt{\frac{(2\ell+1)(\ell-m)!}{4\pi(\ell+m)!}} \tag{8}$$

where $P_{\ell m}(\cos(\theta))$ are the associated Legendre polynomials.

The classical Helfrich Hamiltonian describing the bending energy penalty of thin membrane sheets under tension σ is given by

$$H = \int ds \left[\frac{\kappa}{2}\left(\frac{1}{R_1}+\frac{1}{R_2}\right)^2 + \sigma\right] \tag{9}$$

where κ is the bending modulus, and where the Gaussian bending energy has been omitted since the surface integral of the Gaussian curvature contributes a constant, 4π, for any deformed sphere. For small deviations, $u(\Omega) \ll 1$, one can expand the Helfrich Hamiltonian, Eq. (9), to quadratic order in u_{lm}'s leading to

$$H = \frac{1}{2}\kappa \sum_{\ell\geq 2,m} (\ell-1)(\ell+2)(\ell(\ell+1)+\bar{\sigma})|u_{\ell m}|^2 \tag{10}$$

where $\bar{\sigma} = \sigma R^2/\kappa$ is the reduced membrane tension. Depending on the method by which vesicles are prepared, σ can vary significantly; however, for equilibrium conditions, $\bar{\sigma} \simeq 0$.

Using the equipartition theorem, the amplitude spectrum of the spherical harmonic modes is given by (Milner and Safran [10])

$$\langle u_{\ell m} u^*_{\ell' m'}\rangle = \frac{(k_B T/\kappa)}{(\ell+2)(\ell-1)\Big(\ell(\ell+1)+\bar{\sigma}\Big)}\delta_{\ell\ell'}\delta_{mm'} \tag{11}$$

showing a mean square amplitude that is independent of m, $\langle|u_\ell|^2\rangle \equiv \langle|u_{\ell m}|^2\rangle$. The (relative) equilibrium roughness, $\langle u^2\rangle$, then follows

$$\langle u^2\rangle = \frac{1}{4\pi}\sum_{l=2}^{\ell_{max}} (2\ell+1)\langle|u_\ell|^2\rangle \tag{12}$$

which, for tensionless membranes ($\bar{\sigma} = 0$) and large vesicles ($l_{max} \to \infty$), can be evaluated exactly to give

$$\langle u^2\rangle = \frac{1}{12\pi}\frac{k_B T}{\kappa}. \tag{13}$$

When the decomposition of the membrane into two monolayer leaflets is ignored and the Navier–Stokes equations inside and outside the vesicle are used with appropriate boundary conditions, one obtains the relaxation rate of a mode amplitude u_{lm} in the form [38–40]

$$\omega_{\ell m} = \frac{\kappa}{\eta_{\text{out}} R^3} \frac{(\ell-1)\ell(\ell+1)(\ell+2)\,(\ell(\ell+1)+\bar{\sigma})}{(2\ell^3+3\ell^2+4)+(2\ell^3+3\ell^2-5)\lambda+(4\ell^2+4\ell-8)\,\chi_s}, \tag{14}$$

where $\chi_s = \eta_{\text{mem}}/R\eta_{\text{out}}$ (where η_{mem} is the membrane viscosity) is the ratio of the Saffman-Delbrück length to the vesicle radius, making a dimensionless membrane viscosity parameter, and $\lambda = \eta_{\text{in}}/\eta_{\text{out}}$ is the ratio of viscosities of the solutions inside and outside the vesicle. For identical inside and outside viscosities, $\eta_{\text{in}} = \eta_{\text{out}} \equiv \eta$, and negligible membrane viscosity ($\chi_s \ll 1$), the result for the relaxation rate reduces to the one reported by Milner and Safran [10],

$$\omega_{\ell m} = \frac{\kappa}{\eta R^3}\frac{(\ell-1)\ell(\ell+1)(\ell+2)\,(\ell(\ell+1)+\bar{\sigma})}{4\ell^3+6\ell^2-1}. \tag{15}$$

Note that $\omega_{\ell m}$ are degenerate in m. Langevin dynamics of the normal modes leads to the following mode autocorrelation function

$$\langle u_{lm}(t) u_{l'm'}(0)^*\rangle = \frac{(k_B T/\kappa)\delta_{ll'}\delta_{mm'}}{(l+2)(l-1)\Big(l(l+1)+\bar{\sigma}\Big)}\, e^{-\omega_{\ell m} t}. \tag{16}$$

Accounting for the dynamics of the two monolayer leaflet densities result in a double-exponential autocorrelation function. In general, we may expect that

more detailed models that include other membrane degrees of freedom that couple to the curvature (e.g., tail tilt) will lead to

$$\langle u_{lm}(t)u_{l'm'}(0)^*\rangle = \frac{(k_BT/\kappa)\delta_{ll'}\delta_{mm'}}{(l+2)(l-1)\Big(l(l+1)+\bar{\sigma}\Big)} \sum_i A_i(\ell)e^{-\gamma_i(\ell)t} \tag{17}$$

where $\{\gamma_i(\ell)\}$ are relaxation rates and $\{A_i(\ell)\}$ are amplitudes obeying $\sum_i A_i(\ell) = 1$. In particular, in the spherical adaptation [28] of the Seifert-Langer theory [25,26], there are two independent modes of relaxation, the conventional undulation mode and a slower, compression-expansion mode associated with the fluctuations of the density difference between leaflets.

2.2 Dynamic structure factor of a single vesicle

We proceed now to write the dynamic structure factor of the single vesicle of radius R, assuming *coherent scattering* on the scale of the vesicle. The case of absolute incoherent scattering, likely less relevant for the vesicle sizes studied by NSE since the coherence length is $\gtrsim$ 40 nm, will be mentioned briefly in the Supporting Information (Sect. S1).

Let us start with the definition for the DSF of the single "object" (e.g., macromolecule, vesicle, etc.) [14]

$$\tilde{S}(q,t) = \frac{1}{N}\sum_{i,j}\left\langle e^{i\vec{q}\cdot(\vec{r}_i(t)-\vec{r}_j(0))}\right\rangle \tag{18}$$

where $\vec{r}_i(t)$ is the vector position of molecule i at time t, N is the number of molecules in the vesicle, and we have chosen for convenience the normalization $1/N$. Transforming the two sums in Eq. (18) to integrals over the area, and accounting for the two monolayer leaflets building up the bilayer membrane, we get

$$\tilde{S}(\vec{q},t) = \frac{1}{2\pi R^2 a}\int ds \int ds' \left\langle e^{i\vec{q}\cdot(\vec{r}(\vec{s},t)-\vec{r}(\vec{s}',0))}\right\rangle \tag{19}$$

where a is the area per lipid/surfactant molecule (such that $N = 8\pi R^2/a$), and $\vec{s}$ is a 2D surface vector. Choosing, for convenience (but without loss of generality), the scattering wavevector $\vec{q}$ in the positive z-direction, and defining for convenience $\tilde{S}(\vec{q},t) = \frac{2\pi R^2}{a}S(\vec{q},t)$, we arrive at the following formal expression

$$\begin{aligned} S(\vec{q},t) &= \frac{1}{4\pi^2}\int d\Omega \int d\Omega' \left\langle e^{i\vec{q}\cdot(\vec{r}_s(\Omega,t)-\vec{r}_s(\Omega',0)}\right\rangle \\ &= \frac{1}{4\pi^2}\int d\Omega \int d\Omega' e^{iqR\left(\cos\theta-\cos\theta'\right)} \\ &\quad\times\left\langle e^{iqR(\cos\theta\, u(\Omega,t)-\cos\theta' u(\Omega',0))}\right\rangle \end{aligned} \tag{20}$$

where $\Omega = (\theta,\phi)$ and $\Omega' = (\theta',\phi')$ are 3D angles, $\int d\Omega \equiv \int_0^\pi d\theta\sin\theta \int_0^{2\pi} d\phi$, and we have used Eq. (5) for $\vec{r}_s(\Omega)$. Due to the Gaussian property of the fluctuations $u(\Omega,t)$, and similar to the case of flat membranes, the average in Eq. (20) can be performed explicitly, yielding

$$S(\vec{q},t) = \frac{1}{4\pi^2}\int d\Omega \int d\Omega' e^{iqR(\cos\theta-\cos\theta')}e^{-\frac{R^2q^2}{2}f(\Omega,\Omega',t)} \tag{21}$$

where

$$\begin{aligned} f(\Omega,\Omega',t) &= (\cos^2\theta+\cos^2\theta')\langle u^2\rangle \\ &\quad -2\cos\theta\cos\theta'\langle u(\Omega,t)u(\Omega',0)\rangle \end{aligned} \tag{22}$$

or, equivalently,

$$\begin{aligned} f(\Omega,\Omega',t) &= (\cos\theta-\cos\theta')^2\langle u^2\rangle \\ &\quad +\cos\theta\cos\theta'\langle(u(\Omega,t)-u(\Omega',0))^2\rangle. \end{aligned} \tag{23}$$

The $e^{iqR\left(\cos\theta-\cos\theta'\right)}$ term alone in the integrand of Eq. (21) would give rise to the SSF of a rigid, non-fluctuating, spherical shell, $S(q) = 4\sin^2(qR)/(qR)^2$.

To evaluate the two-point MSD, $\langle(u(\Omega,t)-u(\Omega',0))^2\rangle$, we now make use of Eqs. (6) and (16), and the so-called addition theorem of the spherical harmonics (Ref. [41], Eq. (3.62))

$$\sum_{m=-\ell}^{\ell} Y_{\ell m}(\Omega)Y^*_{\ell m}(\Omega') = \frac{(2\ell+1)}{4\pi}P_\ell(\cos\gamma)$$

where $P_\ell(\cos\gamma)$ are Legendre polynomials, and γ is the 3D angle between Ω and Ω', that obeys

$$\cos\gamma = \cos\theta\cos\theta' + \sin\theta\sin\theta'\cos(\phi-\phi'). \tag{24}$$

This leads to the following two-point correlation function

$$\left\langle(u(\Omega,t)u(\Omega',0))\right\rangle = \frac{1}{4\pi}\sum_{\ell=2}^{\ell_{max}}(2\ell+1)\langle|u_\ell|^2\rangle P_\ell(\cos\gamma)e^{-\omega_\ell t} \tag{25}$$

and so to the two-point MSD

$$\begin{aligned} &\left\langle(u(\Omega,t)-u(\Omega',0))^2\right\rangle \\ &= \frac{1}{2\pi}\sum_{\ell=2}^{\ell_{max}}(2\ell+1)\langle|u_\ell|^2\rangle\left(1-P_\ell(\cos\gamma)e^{-\omega_\ell t}\right). \end{aligned} \tag{26}$$

In particular, the single point MSD ($\Omega = \Omega'$, implying $\gamma = 0$) is

$$\langle \Delta u^2(t) \rangle = \frac{1}{2\pi} \sum_{\ell=2}^{\ell_{max}} (2\ell+1) \langle |u_\ell|^2 \rangle (1 - e^{-\omega_\ell t}). \tag{27}$$

For tensionless and sufficiently large vesicles—i.e., giant unilamellar vesicles (GUVs) with radii on the order of microns—for which $\ell_{max} \gg 1$, and within a short-time regime, $\tau_0 \ll t \ll \tau_r$, where $\tau_r \approx \eta R^3/\kappa$ is the longest relaxation time and $\tau_0 \approx \eta\delta^3/\kappa$ is the short-time cutoff (more accurately, $\tau_r = \omega_{\ell=2}^{-1}$ and $\tau_0 = \omega_{\ell=\ell_{max}}^{-1}$), $\langle \Delta u^2(t) \rangle$ approaches the familiar anomalous subdiffusion (asymptotic "ZG") behavior $\sim t^{2/3}$,

$$\langle \Delta u^2(t) \rangle_{\rm ZG} = \frac{\Gamma[1/3]}{2\pi 4^{2/3}} \frac{k_B T}{R^2 \eta^{2/3} \kappa^{1/3}} t^{2/3}. \tag{28}$$

For $t \to \infty$, or effectively $t \gtrsim \tau_r$, such that $\mathrm{e}^{-\omega_\ell t} \approx 0$ for all ℓ, the MSD saturates at the value $2\langle u^2 \rangle$, *c.f.* Eqs. (12) and (13).

Because the longest relaxation time (determined by the $\ell = 2$ mode) strongly depends on R, $\tau_r \propto R^3$, the fluctuations will fully relax and the MSD will saturate at shorter times in smaller vesicles. In Fig. 1, we compare the dimensioned MSD,$\langle \Delta h^2(t) \rangle \equiv R^2 \langle \Delta u^2(t) \rangle$, calculated using Eq. (27) to the asymptotic $t^{2/3}$ behavior (Eq. (28)), to highlight these effects in small vesicles in the NSE time window. The MSD for the small vesicles follows the $t^{2/3}$ scaling up to ≈ 10 ns, which is why the asymptotic ZG stretched exponential expression described NSE data reasonably well when it was first published and the maximum accessible Fourier time was ≈ 40 ns. Deviations from the commonly assumed $t^{2/3}$ scaling for R values typical of extruded vesicles become much more pronounced for longer times now accessible on modern NSE spectrometers. Fortunately, the advances in computing power over the past 25 years make it more feasible to numerically integrate the expressions for the DSF to account for the finite-size and spherical geometry effects in NSE data at $t \geq 100$ ns. Also note that the MSD for $R = 30$ nm saturates at $\tau_r \approx 200$ ns, which explains why previous fits of NSE data with an empirical non-relaxed amplitude gave more reasonable estimates κ [17].

Before we proceed further, we present another equivalent form for the two-point correlator $f(\Omega, \Omega', t)$. It may be separated into a purely static correlator and a dynamic, spatiotemporal, correlator, as follows

$$\left\langle (u(\Omega,t) - u(\Omega',0))^2 \right\rangle = \left\langle (u(\Omega) - u(\Omega'))^2 \right\rangle + \Phi(\Omega - \Omega', t) \tag{29}$$

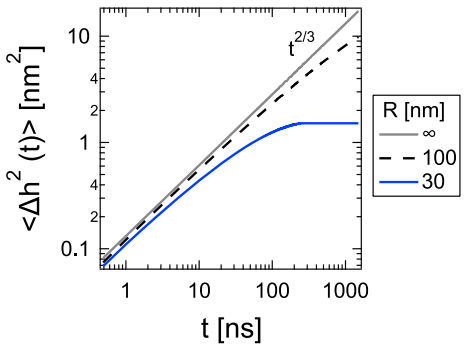

Fig. 1 Comparison of the asymptotic value of the dimensioned mean-squared displacement (MSD), $\langle \Delta h^2(t) \rangle$, for sufficiently large vesicles ($R \to \infty$) that recovers the familiar $t^{2/3}$ scaling with the values calculated as $\langle \Delta h^2(t) \rangle \equiv R^2 \langle \Delta u^2(t) \rangle$ using Eq. (27) for vesicles with $R = 30$ nm and $R = 100$ nm with a bilayer thickness $\delta = 3$ nm, membrane bending modulus, $\kappa = 30$ k_BT, and solvent viscosity, $\eta = 0.001$ Pa s. The spherical geometry and finite size of the vesicles most often studied with NSE result in significant deviations from the commonly assumed $t^{2/3}$ scaling, especially at $t \to 100$ ns, as is routinely accessible on modern NSE spectrometers

where the static correlator, that determines the static structure factor, is

$$\left\langle (u(\Omega) - u(\Omega'))^2 \right\rangle = \frac{1}{2\pi} \sum_{\ell=2}^{\ell_{max}} (2\ell+1) \langle |u_\ell|^2 \rangle \left(1 - P_\ell(\cos\gamma)\right) \tag{30}$$

and the dynamic propagator is

$$\Phi(\Omega - \Omega', t) = \frac{1}{2\pi} \sum_{\ell=2}^{\ell_{max}} (2\ell+1) \langle |u_\ell|^2 \rangle P_\ell(\cos\gamma) \left(1 - \mathrm{e}^{-\omega_\ell t}\right). \tag{31}$$

For completeness, in the Supporting Information, Sect. S1, we provide a few limiting expressions for the DSF, Eq. (21), corresponding to (i) ideal incoherent scattering (Sec. S1.1), that is not typically applicable however to NSE, (ii) small undulation amplitude limit for which the Milner-Safran expression was developed [10] (Sec. S1.2), (iii) quasi-flat membrane limit for which the ZG formula was advanced [11,12].

We note in passing that, in case of additional modes other than bending and membrane viscosity controlling the dynamics (such as the spherically generalized Seifert-Langer modes [25,26,28]), c.f. Equation (17), the two-point correlator will take the form

$$\left\langle (u(\Omega,t) - u(\Omega',0))^2 \right\rangle = \frac{1}{2\pi} \sum_{\ell=2}^{\ell_{max}} (2\ell+1) \langle |u_\ell|^2 \rangle \left(1 - P_\ell(\cos\gamma) \sum_i A_i(\ell) \mathrm{e}^{-\gamma_i(\ell) t}\right). \tag{32}$$

2.3 Polydisperse SUVs and LUVs: a useful approximation

While the integral (Eq. 21) can be evaluated numerically for any value of $\vec{q}$, this evaluation is highly computationally time exhaustive. This is especially a problem when a parameter fit is required, such as for interpreting NSE and other dynamic scattering data. Thus, it is worth putting forward approximate expressions that can replace the exact evaluation even for small vesicles.

In the Supporting Information (Sects. S2 and S3), we combine analytical arguments with extensive numerical analyses to deduce a useful approximation to Eq. (21) that is applicable for typical vesicular systems with polydispersity in the range of 15% to 30% of relative (to R) standard deviation. Such polydispersity, in fact, improves substantially the accuracy of the approximation described below, as it smears out the rigid sphere "Bragg oscillations" appearing in the SSF of a monodisperse system. For a mono-disperse system and near the nodes of the SSF, occurring at $qR = n\pi$ (n integer), the errors become too large. Conversely, for the typical polydispersity considered we find

$$\langle S(q,t)\rangle_w \simeq \left\langle S(q)\mathrm{e}^{-(1/2)q^2R^2\langle\Delta u^2(t)\rangle}\right\rangle_w \qquad (33)$$

where $S(q)$ is the vesicle SSF and $\langle ...\rangle_w$ implies a "weight-average" over vesicle size, accounting for a number of scatterers in a vesicle, which is proportional to its area. We also find that it is sufficiently accurate to use in Eq. (33), instead of the complete expression for an undulating spherical vesicle that is rather complicated, the equivalent expression for a thin and rigid spherical shell, $S(q) \simeq 4\frac{\sin^2(qR)}{q^2R^2}$. The overall error for the time and wavenumber regimes relevant to NSE and typical vesicular size range of 20 nm to 400 nm remains mostly within 2%, which is smaller than the typical experimental error.

Given that the center-of-mass diffusion may influence the decay profile within the NSE time window, despite the high-q regime, and that it acquires an R-dependence *via* the Stokes-Einstein relation $D \sim 1/R$ (where D is the diffusion coefficient), Eq. (33) needs to be replaced by [11,12,14]

$$\langle S(q,t)\rangle_w \simeq \left\langle S(q)\mathrm{e}^{-(1/2)q^2R^2\langle\Delta u^2(t)\rangle}\mathrm{e}^{-q^2Dt}\right\rangle_w . \qquad (34)$$

Equation (34) is the concluding theoretical result of this paper and the starting point for numerical fitting procedures to the experimental NSE data described in the next section. In the limit $R \to \infty$, or in terms of dimensionless physical parameters, $\ell_{max} \simeq \pi R/\delta \gg 1$ and $\eta\delta^3/\kappa \ll t \ll \eta R^3/\kappa$, and for vanishing membrane viscosity, it reduces exactly to the ZG stretched exponential asymptotic that is governed by the transverse MSD, $\langle S(q,t)\rangle_w \simeq \langle S(q)\rangle_w \exp\left[-(\Gamma_q t)^{2/3}\right]$. We also note that the full expression, Eq. (34), coincidentally yields roughly the same relaxation as the original asymptotic stretched exponential expression *without* diffusion (Supplementary Information, Fig. S14). In other words, the contributions from the vesicle diffusion and the saturation of the membrane fluctuations at long times combine to give a relaxation that looks similar to the $t^{2/3}$ scaling, which explains why NSE data for small vesicles have historically been found to agree with the scaling predicted for planar membrane plaquettes (i.e. the original ZG scaling).

3 Experiment: NSE measurements of polydisperse LUVs with varying R

3.1 Materials and methods

Lipids were purchased as chloroform solutions from Avanti Polar Lipids and used as received. Appropriate volumes of the 1-palmitoyl-2-oleoyl-glycero-3-phos phocholine (16:0–18:1 PC, POPC) and 1-palmitoyl-2-oleoyl-sn-glycero-3-phospho-L-serine (sodium salt) (16:0–18:1 PS, POPS) stock solutions were mixed such that the lipid mixture contained a mole fraction of 10 % (10 mol %) POPS. The chloroform was removed under a stream of nitrogen gas, and the lipid film was then dried under vacuum overnight to remove any residual solvent. A suspension of multilamellar vesicles (MLV) was prepared by hydrating the dried lipid film with deuterium oxide (99.9 %D, D_2O, Cambridge Isotopes) to a concentration of 20 mg of lipid per mL of D_2O. All samples were prepared using the same MLV stock solution.

Large unilamellar liposomes (LUVs) were prepared by extruding the MLV suspension at room temperature using the handheld Avanti mini extruder. The stock solution was diluted to 5 mg/mL and 10 mg/mL with D_2O before extrusion to prepare the 400 nm and 200 nm samples, respectively, and the MLV suspension was then extruded through the corresponding filters for a total of 21 passes. The 100 nm and 50 nm LUVs were prepared by first extruding the 20 mg/mL MLV suspension through a 200 nm filter a total of 15 times and then subsequently passing the solution through either the 100 nm or 50 nm filter for 21 passes. All solutions were stored at room temperature before use. All measurements were performed at 25 °C.

NSE measurements were performed on the instrument IN15 at the Institut Laue-Langevin (ILL) in Grenoble, France using neutron wavelengths (λ) of 13.5 Å, 12 Å, 10 Å and 8 Å at scattering angles Θ of 3.5°, 6°, 7.5°, and 8.5°, respectively, covering a combined q-range from 0.02 $Å^{-1}$ to 0.13 $Å^{-1}$. The data presented in the paper have been corrected for the instrument resolution and background solvent using standard procedures.

SANS measurements were performed on the instrument D22 at ILL using neutron wavelengths of $\lambda = 6$ Å with the detector carriages positioned at 1.4 m and 17.6 m to collect data over a combined q range from

0.003 Å^{-1} to 0.64 Å^{-1}. Data were reduced using the standard procedures provided by the beamline and analyzed using the vesicle form factor model in SasView. The data were fit assuming a Gaussian distribution of vesicle sizes with a standard deviation of $s \approx 0.3R_0$ (Table 1) [42,43].

Dynamic light scattering (DLS) measurements were also performed using a Malvern ZS90 instrument to determine the diffusion coefficient at infinite dilution (D_0) and corresponding hydrodynamic radii (R_H) of the samples. The samples were diluted with D_2O to lipid concentrations $\leq$ 1 mg/mL, and DLS data for at least three different lipid concentrations were collected for each vesicle size. D_0 was determined by linear extrapolation of the measured diffusion coefficients to a concentration of 0 mg/mL and was used to calculate R_H using the Stokes-Einstein equation, $R_H = \frac{k_B T}{6\pi\eta D_0}$.

The sizes of the vesicles after extrusion and other relevant sample information are summarized in Table 1. We refer to the samples in the results section based on the mean radius (R_0) of the Gaussian distribution of radii that best fit the SANS data.

3.2 Results and discussion

To test the predictions of Eq. (34), we prepared mixed POPC/POPS lipid vesicles that were extruded to different sizes ranging from $R_0 \approx 30$ nm to ≈ 100 nm. In the q range measured with NSE, 0.02 Å$^{-1} \lesssim q \lesssim$ 0.13 Å^{-1} these vesicles sizes correspond to $qR \gg 1$ such that the measurements are expected to be sensitive to the single membrane thermal undulation dynamics. POPC was selected as a model system as it is a widely studied lipid and there are values of κ from different characterization methods with which we can directly compare the present NSE results (Table 2) [45–47]. The incorporation of a small amount of charged POPS lipid ensured that the extruded vesicles were unilamellar [48], as the presence of multilamellar vesicles would complicate the interpretation of the NSE data [49,50]. The samples were also diluted to an effective vesicle volume fraction (ϕ_V, Table 1) less than 0.1 to minimize potential effects of direct and indirect, solvent-mediated interactions between vesicles on the NSE data as these interactions could impact both the membrane undulations [51] and the vesicle diffusion [18,52–54].

3.2.1 SANS: determination of R_0 and s

SANS is a common technique to measure the SSF of small vesicles and extract information about the bilayer structure as well as the overall vesicle size and size distribution. In Fig. 2 we show SANS curves measured for the different vesicle samples normalized by the lipid concentration (ϕ_{lipid}). Importantly, the data at $q \gtrsim 0.03$ Å^{-1}, corresponding to the q range measured with NSE, overlapped and was well described with a model for unilamellar vesicles. The fit value of the bilayer thickness, $\delta = 3.8$ nm $\pm$ 0.1 nm, also agreed well with the value for POPC bilayers in literature [44].

Complementary SANS measurements are especially important, as a precisely determined size distribution of the vesicles is required to obtain reliable values of the bending rigidity through Eq. (34). The lack of sharp oscillations at $q \lesssim 0.01$ Å^{-1} is indicative of a polydisperse population of vesicles and is typical of samples prepared by extrusion. We note that while SANS data fit equally well with either a Gaussian or Schulz distribution of vesicle radius, analysis of microscopy images of extruded vesicles suggested that the distribution was roughly Gaussian [43]. Therefore, the presented analyses all assume a Gaussian distribution of vesicle sizes with a standard deviation, $s/R_0 \approx 0.3$ (Table 1). The corresponding size distributions are shown in Fig. 2.

3.2.2 NSE: measurement of membrane undulation dynamics

It is important to consider the effect of the center-of-mass diffusion of vesicles in NSE data analysis, especially now that modern NSE spectrometers can easily reach up to a few 100 ns in Fourier time. Even for a relatively large vesicle with a radius of 100 nm at $q = 0.05$ Å^{-1} and a maximum Fourier time of 300 ns (which would correspond to a measurement with 12 Å neutrons on IN15) at room temperature, $S(q,t)$ would decay to 0.86, and for smaller vesicles with a radius of 50 nm, the decay would be as low as 0.74 (See Supporting Information, Sect. S4.1). These effects may be comparable, or even greater than, the contribution from the membrane fluctuations at long times (Supplementary Information, S4.1).

It can also be important to take into account the effects of interactions between vesicles on diffusion when analyzing NSE data. NSE samples are often highly concentrated to improve the signal-to-noise ratio and minimize the required measurement times. At the high concentrations, direct (described by the structure factor, $S(q)$) and indirect, solvent-mediated hydrodynamic interactions (referred to as the hydrodynamic factor $H(q)$) impact particle diffusion. These effects have been seen in NSE studies of proteins [63], micelles [52] and vesicles [18]. The effects can be even more pronounced in lipid vesicles because the majority of the vesicle volume is made up of solvent, and seemingly low lipid concentrations can correspond to higher than expected effective vesicle volume fraction (ϕ_V). Here, the lipid vesicle solutions were diluted such that $\phi_v < 0.1$ (Table 1) to minimize the effects of the interactions between vesicles on the NSE data. The SANS curves for all vesicle sizes overlapped and confirmed that $S(Q) = 1$ in the q range measured with NSE (Fig. 2). Likewise, $H(q) \approx 1$ for $\phi_V < 0.1$ so that the vesicle diffusion contribution to the NSE data should be reasonably well described by D_0 as calculated from the vesicle size distribution [53,54].

However, simple multiplication of Eq. (1) with a distribution of diffusion coefficients calculated through the Stokes-Einstein equation $D = \frac{k_B T}{6\pi\eta R_H}$ based on the size distribution obtained from SANS does not lead to sat-

Table 1 Summary of sample properties

Filter pore size (nm)	ϕ^1_{lipid}	R_0(nm) SANS	s/R_0	ϕ^2_V	R_H (nm) DLS
400	0.005	98.3 ± 2.1	0.30	0.04	99.2 ± 2.3
200	0.01	78.1 ± 1.5	0.30	0.07	80.3 ± 1.6
100	0.02	48.1 ± 0.5	0.30	0.08	56.5 ± 0.5
50	0.02	29.7 ± 0.5	0.28	0.05	40.9 ± 0.5

Uncertainties represent one standard deviation estimated from the curve fits
[1]Volume fraction of lipid in D_2O
[2]Effective vesicle volume fraction calculated from ϕ_{lipid}, reported molecular volume of POPC [44], and R_0 and δ values from the fits to the SANS data

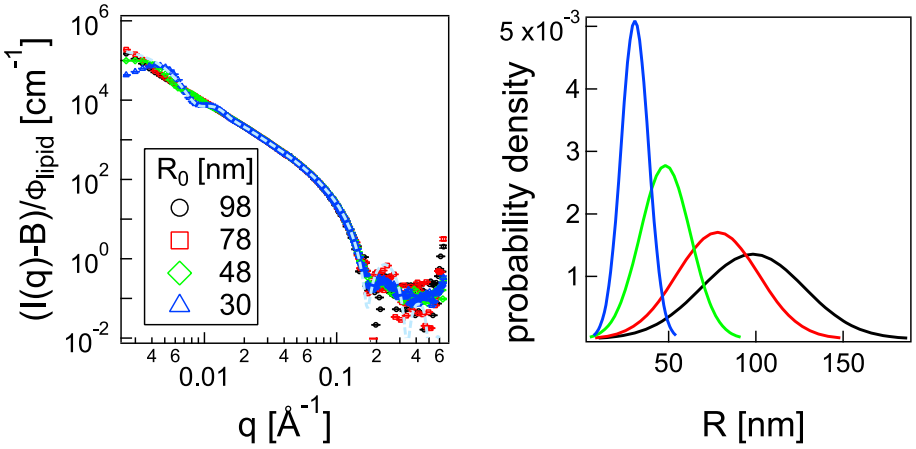

Fig. 2 Left: Normalized SANS data (symbols) where $I(q)$ is the measured intensity, B is the incoherent background estimated from the data at high Q and ϕ_{lipid} is the lipid volume fraction (Table 1). The dashed line is the fit to the data for $R = 30$ nm sample to a unilamellar vesicle form factor assuming a Gaussian distribution of vesicle sizes. Error bars on the SANS data represent one standard deviation. The form factor fits to the other samples are not shown for clarity. Right: Corresponding normalized Gaussian distributions of vesicle sizes from fits to the SANS data

Table 2 Summary of values of κ and K_A from fluctuation analysis (FA), electro-deformation (ED), X-ray diffuse scattering (XDS), simulations (SIM), and micropipette aspiration (MA) for POPC at $T = 25$ °C

κ (k_BT)					K_A (mN m^{-1})			d (nm)	$\tilde{\kappa}$ (k_BT)[a]
FA	ED	XDS	SIM	Average	MA	SIM	Average		
8.5 ± 1.9[b]	12.0 ± 2.2[c]	30.7 ± 2.5[d]	24.3 ± 0.9[e]	25.2	213 ± 5[f]	240 ± 10[g]	244	1.45[h]	150 ± 36
28.0 ± 3.6[i]	13.1 ± 2.6[b]		36.5 ± 1.1[g]			280 ± 10[g]			
34.5 ± 0.7[j]									
38.5 ± 0.8[k]									

The uncertainties are the values reported in literature or the propagated standard deviation for any calculated values. Note values reported at different temperatures were adjusted to 25 ° C using the reported temperature dependence of κ of 0.995/°C [55]
[a]The literature value of $\tilde{\kappa}$ was calculated using the average values of κ and K_A per Eq. (4) assuming $2K_m = K_A$ [56].
[b]Niggemann, Kummrow, and Helfrich [57]
[c]Faizi, Dimova and Vlahovska [28]
[d]Nagle [46]
[e]Doktorova, Harries, and Khelashvili [58]
[f]Henriksen et al. [59]
[g]Venable, Brown and Pastor [60]
[h]d is assumed to be located at the interface of the hydrocabon tails and hydrophilic headgroup, $d = D_c$, and the hydrocarbon thickness of the monolayer D_C was taken from Kučerka, Nieh, and Katsaras [44]
[i]Faizi et al. [47]
[j]Bouvrais, Duelund, and Ipsen [61]
[k]Henriksen and Ipsen [62]

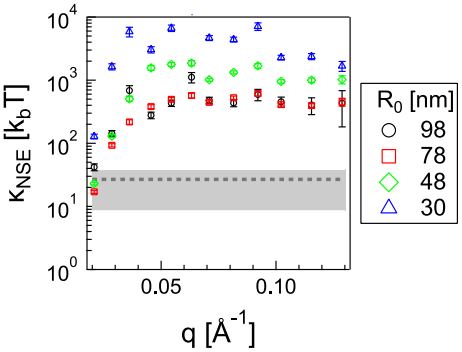

Fig. 3 Bending rigidities obtained from fitting the NSE data with the asymptotic ZG stretched exponential expression Eq. (1) multiplied with a distribution of diffusion coefficients obtained from SANS as a function of q for differently sized vesicles. The extracted κ_{NSE} values strongly depend on the size of the vesicles, and the values of the bending rigidity for the 30 nm and 48 nm are unrealistically high. The gray shaded region shows the range of κ values reported for POPC in literature (Table 2), and the dashed line is the average of the reported κ values. Error bars represent one standard deviation and were estimated from the Least Squares fit to the data

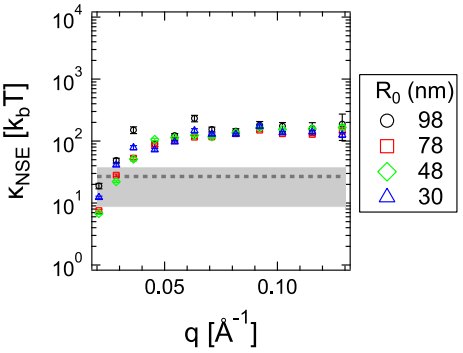

Fig. 4 Results obtained for κ_{NSE} using Eq. (34) and diffusion coefficients calculated based on R_0 and s values from SANS. Error bars represent one standard deviation and were estimated from the Least Squares fit to the data. The κ_{NSE} value for different vesicle sizes nicely coincide, though the obtained fit values decrease at $q < 0.06$ Å^{-1}

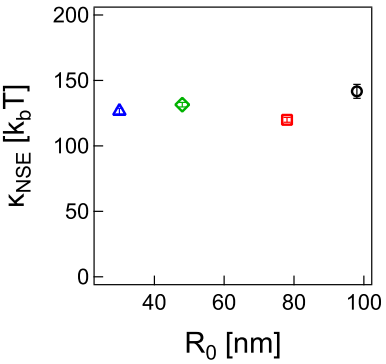

Fig. 5 Values of κ_{NSE} as a function of R_0 obtained from fits of the NSE data between 0.06 Å^{-1} and 0.13 Å^{-1} with Eq. (34). Importantly, the extracted κ_{NSE} values are quite constant regardless of the vesicle size. Error bars represent one standard deviation and were estimated from the Least Squares fit to the data

isfactory results in the sense that the values of the bending modulus extracted from the NSE data (κ_{NSE}) depend on the size of the vesicles (see Fig. 3). The extracted values of κ_{NSE} are also on the order of 1000 k_BT, two order of magnitude larger than values of κ in literature (Table 2) and an order of magnitude larger than expected values of the effective bending modulus, $\tilde{\kappa} \approx 100\ k_bT$ [16,25,26]. Even adopting assumptions relating $\tilde{\kappa}$ and κ, that instead of a prefactor value $\left(\frac{\Gamma[1/3]}{4\pi 4^{2/3}}\right)^{3/2} \approx 0.025$ given by Eq. (2), give a prefactor value of 0.0069 [30], result in κ values upwards of 300 k_BT for the 30 nm vesicle. While the incorporation of charged lipids is known to make membranes more rigid, theoretical and experimental studies have shown that charge changes the membrane properties by approximately 10% [47,64,65], not orders of magnitude as seen in the κ_{NSE} values in Fig. 3. The unrealistically large values of κ, and even $\tilde{\kappa}$, seem to suggest that the stretched exponential function given by Eq. (1) and derived for the asymptotic limit of giant vesicles does not work for small unilamellar vesicles with $R_0 \approx 50$ nm to 100 nm.

By comparison, using Eq. (34) with the size distribution from SANS gives very satisfactory results in that the extracted κ_{NSE} values do not depend on the size of the vesicle (see Fig. 4).

Quite interestingly though, it can be seen that the κ_{NSE} values decrease at low $q < 0.06$ Å^{-1}, which may mark the limit of validity of our assumptions or potential contributions of other dynamic modes at lower q values and longer times. On a pragmatic level, this is good news for determining values of κ_{NSE} as measurements are only required in a relatively narrow q range where the form factor scales smoothly as q^{-2} with q large enough so that oscillations due to the overall size are not visible and q small enough so that oscillations due to the finite thickness of the membrane do not come into play. For the usual lipid vesicle, this corresponds to a q range from about 0.05 Å^{-1} to 0.15 Å^{-1} and coincidentally, this is a q range where NSE measurements are relatively fast and easy. The low q limit of 0.05 Å^{-1} is high enough that the relaxations are not too slow such that exceedingly long Fourier times are not needed, and the high q limit is sufficiently low so that the scattering intensity is not yet vanishingly small.

Knowing the limitations of the approximation we try to fit our data for each R_0 with a single, q independent κ_{NSE} between from 0.06 Å^{-1} to 0.13 Å^{-1} and obtain quite similar values of around 140 k_BT for the different sizes (see Fig. 5) where only the $R_0 \approx 100$ nm sample gives somewhat larger values. Observing some slight deviations in this sample is not overly surprising as both statistics are worse compared to the other samples due to the lower lipid concentration used in this sample (Table 1) and it was not possible to pre-

cisely determine the size distribution from SANS. We also note that varying the values of R_0 by 10 % at a constant value of s or varying s between 0.1 and 0.3 at a fixed value of R_0 did not significantly change the best fit values of κ_{NSE} (see Supporting information Sect. S4). Pushing the analysis one step further, we obtain good fits when simultaneously fitting data for all samples with a single value of κ_{NSE} (see Fig. 6) which gives $137\pm1\ k_BT$.

This κ_{NSE} value is the same order of magnitude expected $\tilde{\kappa}$ and within 10 % of the value estimated for POPC bilayers calculated using Eq. (4) based on published values of κ and K_A (Table 2). Taking the best fit κ_{NSE} as $\tilde{\kappa}$ and the values in Table 2 for κ and K_A gives $d = 1.36$ nm or $d/2D_c = 0.47$, placing d close to the often-assumed location at the interface between the hydrophobic tails and hydrophilic headgroups. This d value is consistent with some simulation results [60,66,67], though it is important to note that the location of d remains a topic of discussion of in literature with values of $d/2D_c$ ranging from 0.25 to 0.6 [16,60,68–70].

The excellent agreement in the estimated values of $\tilde{\kappa}$ and d values from the NSE experiments and results in literature seems to suggest that NSE does indeed measure the effective bending modulus as first proposed by Watson and Brown [8,9,16]. This agreement is quite promising and indicates that NSE may offer new opportunities to understand how lipid composition and various additives impact $\tilde{\kappa}$ and how changes in $\tilde{\kappa}$ compare with κ values extracted from complementary methods. Moreover, the decrease in κ_{NSE} values at $q < 0.06$ Å^{-1} in Fig. 4 may suggest a transition from "unrelaxed" bending fluctuations dictated by $\tilde{\kappa}$ at high q and short times to "relaxed" bending fluctuations governed by κ at low q and long times as predicted by Seifert and Langer [25,26], though careful NSE measurements over a wider time window would be needed to say for certain.

Alternatively, recent work by Faizi et al. suggests that the membrane viscosity should significantly impact the undulation relaxation dynamics in small unilamellar vesicles with $R \lesssim 50$ nm [28]. Preliminary analysis of the current NSE data accounting for the potential effects of the membrane viscosity gave κ_{NSE} values on the order of 10 k_BT and membrane viscosity values on the order of 1 nPa s m. However, we note that more exploration of the new theoretical predictions for the relative effects of $\tilde{\kappa}$ and membrane viscosity are needed to better understand the potential role of membrane viscosity in the dynamics of small vesicles and will be the focus of a future manuscript.

While the present data alone do not allow us to distinguish between the different proposed mechanisms of dissipation that come into play at the nanoscale (i.e. distinguish between $\tilde{\kappa}$ or potential membrane viscosity effects), the presented analysis clearly shows that it is necessary to account for the finite-size effects in NSE data analysis. Fitting the data with Eq. (34) not only gives the same κ_{NSE} value independent of the vesicle size, but the κ_{NSE} values are consistent with the order of magnitude expected based on current models. Moreover, the *generalized* approximations derived here can be easily extended to other models for the membrane undulations to better understand the relaxation dynamics at nanometer length scales and nanosecond timescales measured with NSE.

4 Summary and conclusions

We have developed a formula for the dynamic structure factor of vesicles, associated with the Helfrich membrane bending undulations, and account for the finite size and spherical geometry of vesicles used in NSE experiments and other scattering methods. The exact expression was simplified to make it practical for common use in experimental data fits. The final approximation, Eq. (34), takes advantage of the polydisperse vesicle size distribution that is very common in experimental samples, even after filtration or vesicle extrusion. The new approximation shows that the contribution of the single-point MSD of the membrane dominates the DSF relaxation profile and approaches the traditional ZG stretched exponential asymptotic expression for sufficiently large vesicles. Our new expression is also general enough to accommodate the dynamics of more degrees of freedom (see Eq. (32)), such as the two leaflet densities, as done by Seifert and Langer [25,26], later used by Watson and Brown to calculate the DSF of quasi-flat membrane plaquettes [8,9,16], and more recently generalized to spherical geometry by Faizi et al [28].

The new expression was tested against NSE experiments on POPC:POPS 90% : 10% (molar ratio) vesicles that were extruded to different sizes with R_0 varying from $\approx$ 30 nm to 100 nm. The NSE data were fitted to Eq. (34) with κ_{NSE} as the only fit parameter. Remarkably, and in contrast to fits with the asymptotic ZG stretched exponential expression commonly used to analyze NSE data, the values of κ_{NSE} obtained from the fits were independent of R_0 as would be expected for a material property of the membrane. Moreover, the extracted κ_{NSE} values were in excellent agreement with estimates for $\tilde{\kappa}$ from the available data on the equilibrium (fully relaxed) bending modulus (κ) and leaflet monolayer compression modulus (Table 2). The good agreement highlights that the new expressions developed here correctly capture the combined finite size and spherical geometry effects in the vesicle samples often studied with NSE and will help provide new insights into the membrane undulation dynamics at the nanoscale.

Supplementary information Please see Supplementary Information included for additional limiting expressions (Sect. S1), approximations and associated relative errors (Sect. S2), calculations of the effects of polydispersity on the center-of-mass diffusion (Sect. S3) and sensitivity analysis of the fits to the NSE data (Sect. S4).

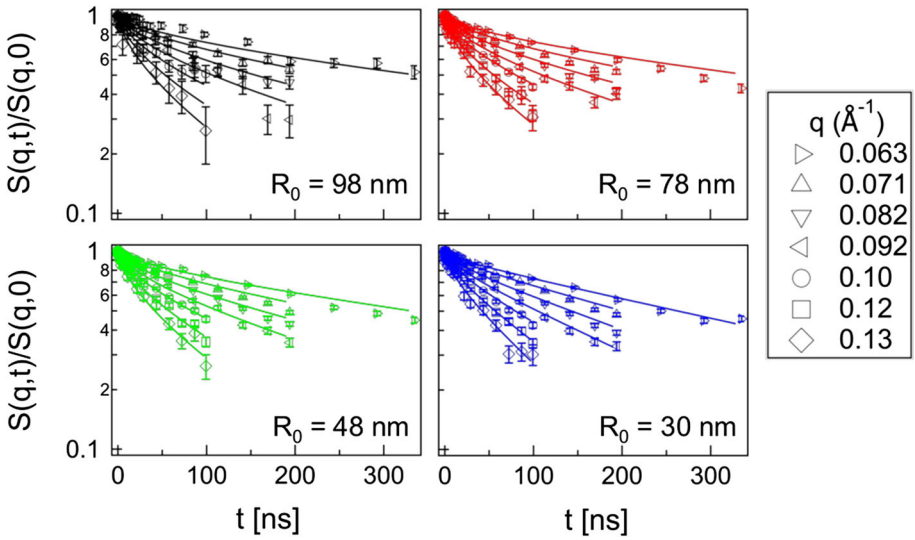

Fig. 6 Measured $S(q,t)/S(q,0)$ (points) and simultaneous fits (lines) to all data for the different vesicle sizes with Eq. 34 and a single value of κ_{NSE}. Note that relatively good fits are obtained for all curves when the vesicle size distribution is taken into account. Error bars on the data represent one standard deviation based on the counting statistics

Supplementary information The online version contains supplementary material available at https://doi.org/10.1140/epje/s10189-023-00400-9.

Acknowledgements The authors gratefully acknowledge Ryan Murphy and Lionel Porcar for assistance with the SANS data collection, and John Nagle for useful discussions. The authors also acknowledge the Partnership for Soft Condensed Matter (PSCM) for providing access to the DLS instrument and laboratory infrastructure used for sample preparation. EGK and MN acknowledge support from the Center for High Resolution Neutron Scattering, a partnership between the National Institute of Standards and Technology (NIST) and the National Science Foundation under Agreement No. DMR-2010792. The identification of any commercial products does not imply endorsement or recommendation by NIST. This work benefited from the use of the SasView application, originally developed under NSF award DMR-0520547. SasView contains code developed with funding from the European Union's Horizon 2002 research and innovation programme under the SINE2020 project, grant agreement No 654000. This research was also supported in part by the National Science Foundation under Grant No. NSF PHY-1748958

Author contribution statement

RG, AZ, and PMV developed the theory. IH, EGK, and MN performed the experiment. RG, IH, EGK, and MN wrote the article.

Data availability Raw data of the experiment are available at doi.ill.fr/10.5291/ILL-DATA.DIR-277.

References

1. É. Freyssingeas, D. Roux, F. Nallet, Quasi-elastic light scattering study of highly swollen lamellar and "sponge" phases. J. Phys. II **7**(6), 913–929 (1997)
2. R. Hirn, T.M. Bayerl, J.O. Rädler, E. Sackmann, Collective membrane motions of high and low amplitude, studied by dynamic light scattering and microinterferometry. Faraday Discuss. **111**, 17–30 (1999). https://doi.org/10.1039/A807883A
3. P. Falus, M. Borthwick, S. Mochrie, Fluctuation dynamics of block copolymer vesicles. Phys. Rev. Lett. **94**(1), 016105 (2005)
4. P. Falus, M. Borthwick, S. Narayanan, A. Sandy, S. Mochrie, Crossover from stretched to compressed exponential relaxations in a polymer-based sponge phase. Phys. Rev. Lett. **97**(6), 066102 (2006)
5. S. Gupta, R. Ashkar, The dynamic face of lipid membranes. Soft Matter **17**(29), 6910–6928 (2021)
6. V. Sharma, E. Mamontov, Multiscale lipid membrane dynamics as revealed by neutron spectroscopy. Prog. Lipid Res. 101179 (2022)
7. M. Nagao, H. Seto, Neutron scattering studies on dynamics of lipid membranes. Biophys. Rev. **4**(2) (2023)
8. M.C. Watson, Y. Peng, Y. Zheng, F.L.H. Brown, The intermediate scattering function for lipid bilayer membranes: from nanometers to microns. J. Chem. Phys. **135**(19), 194701 (2011). https://doi.org/10.1063/1.3657857
9. M.C. Watson, E.S. Penev, P.M. Welch, F.L.H. Brown, Thermal fluctuations in shape, thickness, and molecular orientation in lipid bilayers. J. Chem. Phys. **135**(24), 244701 (2011). https://doi.org/10.1063/1.3660673
10. S.T. Milner, S.A. Safran, Dynamical fluctuations of droplet microemulsions and vesicles. Phys. Rev. A **36**, 4371–4379 (1987). https://doi.org/10.1103/PhysRevA.36.4371
11. A.G. Zilman, R. Granek, Undulations and dynamic structure factor of membranes. Phys. Rev. Lett. **77**(23), 4788–4791 (1996). https://doi.org/10.1103/PhysRevLett.77.4788
12. A.G. Zilman, R. Granek, Membrane dynamics and structure factor. Chem. Phys. **284**(1), 195–204 (2002). https://doi.org/10.1016/S0301-0104(02)00548-7
13. S. Lovesey, P. Schofield, Inelastic coherent neutron scattering by small particles. J. Phys. C Solid State Phys. **9**(15), 2843 (1976)

14. M. Doi, S.F. Edwards, *The Theory of Polymer Dynamics*, vol. 73 (Oxford University Press, Oxford, 1988)
15. P.-G. De Gennes, *Scaling Concepts in Polymer Physics* (Cornell University Press, London, 1979)
16. M.C. Watson, F.H. Brown, Interpreting membrane scattering experiments at the mesoscale: the contribution of dissipation within the bilayer. Biophys. J . **98**(6), 9–11 (2010). https://doi.org/10.1016/j.bpj.2009.11.026
17. I. Hoffmann, Background subtraction and dada analysis in neutron spin echo spectroscopy. Front. Phys. (2021). https://doi.org/10.3389/fphy.2020.620082
18. E.G. Kelley, E.E. Blick, V.M. Prabhu, P.D. Butler, M. Nagao, Interactions, diffusion, and membrane fluctuations in concentrated unilamellar lipid vesicle solutions. Front. Phys. **10**, 288 (2022)
19. M. Monkenbusch, O. Holderer, H. Frielinghaus, D. Byelov, J. Allgaier, D. Richter, Bending moduli of microemulsions; comparison of results from small angle neutron scattering and neutron spin-echo spectroscopy. J. Phys. Condens. Matter **17**(31), 2903–2909 (2005). https://doi.org/10.1088/0953-8984/17/31/017
20. M. Ohl, M. Monkenbusch, N. Arend, T. Kozielewski, G. Vehres, C. Tiemann, M. Butzek, H. Soltner, U. Giesen, R. Achten, H. Stelzer, B. Lindenau, A. Budwig, H. Kleines, M. Drochner, P. Kaemmerling, M. Wagener, R. Möller, E.B. Iverson, M. Sharp, D. Richter, The spin-echo spectrometer at the spallation neutron source (sns). Nucl. Instrum. Methods Phys. Res. Sect. A Accel. Spectrom. Detect. Assoc. Equip. **696**, 85–99 (2012). https://doi.org/10.1016/j.nima.2012.08.059
21. O. Holderer, O. Ivanova, J-nse: neutron spin echo spectrometer. J. Large-scale Res. Facil. JLSRF **1**, 11–11 (2015)
22. B. Farago, P. Falus, I. Hoffmann, M. Gradzielski, F. Thomas, C. Gomez, The in15 upgrade. Neutron News **26**(3), 15–17 (2015). https://doi.org/10.1080/10448632.2015.1057052
23. W. Helfrich, Elastic properties of lipid bilayers: theory and possible experiments. Z. Naturforsch. C **28**, 693–703 (1973)
24. U. Seifert, K. Berndl, R. Lipowsky, Shape transformations of vesicles: Phase diagram for spontaneous-curvature and bilayer-coupling models. Phys. Rev. A **44**(2), 1182 (1991)
25. U. Seifert, S.A. Langer, Viscous modes of fluid bilayer membranes. Europhys. Lett. **23**(1), 71–76 (1993). https://doi.org/10.1209/0295-5075/23/1/012
26. U. Seifert, S.A. Langer, Hydrodynamics of membranes: the bilayer aspect and adhesion. Biophys. Chem. **49**(1), 13–22 (1994). https://doi.org/10.1016/0301-4622(93)E0077-I
27. L.R. Arriaga, R. Rodríguez-García, B. López-Montero, T. Farago, F. Monroy. Hellweg, Dissipative curvature fluctuations in bilayer vesicles: coexistence of pure-bending and hybrid curvature-compression modes. Eur. Phys. J. E **31**(1), 105–113 (2010). https://doi.org/10.1140/epje/i2010-10551-1
28. H.A. Faizi, R. Granek, P.M. Vlahovska, Membrane viscosity signature in thermal undulations of curved fluid bilayers (2022)
29. A.C. Woodka, P.D. Butler, L. Porcar, B. Farago, M. Nagao, Lipid bilayers and membrane dynamics: insight into thickness fluctuations. Phys. Rev. Lett. **109**(5), 058102 (2012)
30. M. Nagao, E.G. Kelley, R. Ashkar, R. Bradbury, P.D. Butler, Probing elastic and viscous properties of phospholipid bilayers using neutron spin echo spectroscopy. J. Phys. Chem. Lett. **8**(19), 4679–4684 (2017). https://doi.org/10.1021/acs.jpclett.7b01830
31. R.J. Bingham, S.W. Smye, P.D. Olmsted, Dynamics of an asymmetric bilayer lipid membrane in a viscous solvent. EPL **111**(1), 18004 (2015). https://doi.org/10.1209/0295-5075/111/18004
32. R. Granek, Comment on "dynamics of phospholipid membranes beyond thermal undulations". J. Phys. Chem. B **123**(26), 5665–5666 (2019). https://doi.org/10.1021/acs.jpcb.9b03049
33. L. Moleiro, M. Mell, R. Bocanegra, I. López-Montero, P. Fouquet, T. Hellweg, J. Carrascosa, F. Monroy, Permeability modes in fluctuating lipid membranes with DNA-translocating pores. Adv. Coll. Interface. Sci. **247**, 543–554 (2017)
34. R. Granek, Membrane surrounded by viscoelastic continuous media: anomalous diffusion and linear response to force. Soft Matter **7**(11), 5281–5289 (2011)
35. R. Granek, H. Diamant, Membrane undulations in a structured fluid: universal dynamics at intermediate length and time scales. Eur. Phys. J. E **41**, 1–10 (2018)
36. M. Schneider, J. Jenkins, W. Webb, Thermal fluctuations of large quasi-spherical bimolecular phospholipid vesicles. J. Phys. **45**(9), 1457–1472 (1984)
37. K. Seki, S. Komura, Viscoelasticity of vesicle dispersions. Phys. A **219**(3–4), 253–289 (1995)
38. P. Olla, The behavior of closed inextensible membranes in linear and quadratic shear flows. Phys. A **278**(1–2), 87–106 (2000)
39. S. Rochal, V. Lorman, G. Mennessier, Viscoelastic dynamics of spherical composite vesicles. Phys. Rev. E **71**(2), 021905 (2005)
40. P.M. Vlahovska, Electrohydrodynamics of drops and vesicles. Annu. Rev. Fluid Mech. **51**, 305–330 (2019)
41. J.D. Jackson, *Classical Electrodynamics* (Wiley, New York, 1998)
42. M. Hope, M. Bally, G. Webb, P. Cullis, Production of large unilamellar vesicles by a rapid extrusion procedure characterization of size distribution, trapped volume and ability to maintain a membrane potential. Biochim. Biophys. Acta (BBA) Biomembr. **812**(1), 55–65 (1985)
43. A.H. Kunding, M.W. Mortensen, S.M. Christensen, D. Stamou, A fluorescence-based technique to construct size distributions from single-object measurements: application to the extrusion of lipid vesicles. Biophys. J. **95**(3), 1176–1188 (2008)
44. N. Kučerka, M.-P. Nieh, J. Katsaras, Fluid phase lipid areas and bilayer thicknesses of commonly used phosphatidylcholines as a function of temperature. Biochim. Biophys. Acta (BBA) Biomembr. **1808**(11), 2761–2771 (2011). https://doi.org/10.1016/j.bbamem.2011.07.022
45. R. Dimova, Recent developments in the field of bending rigidity measurements on membranes. Adv. Colloid Interface Sci. **208**, 225–234 (2014). https://doi.org/10.1016/j.cis.2014.03.003
46. J.F. Nagle, Experimentally determined tilt and bending moduli of single-component lipid bilayers. Chem. Phys.

Lipids **205**, 18–24 (2017). https://doi.org/10.1016/j.chemphyslip.2017.04.006
47. H.A. Faizi, S.L. Frey, J. Steinkühler, R. Dimova, P.M. Vlahovska, Bending rigidity of charged lipid bilayer membranes. Soft Matter **15**(29), 6006–6013 (2019). https://doi.org/10.1039/C9SM00772E
48. H.L. Scott, A. Skinkle, E.G. Kelley, M.N. Waxham, I. Levental, F.A. Heberle, On the mechanism of bilayer separation by extrusion, or why your luvs are not really unilamellar. Biophys. J. **117**(8), 1381–1386 (2019). https://doi.org/10.1016/j.bpj.2019.09.006
49. H. Seto, N.L. Yamada, M. Nagao, M. Hishida, T. Takeda, Bending modulus of lipid bilayers in a liquid-crystalline phase including an anomalous swelling regime estimated by neutron spin echo experiments. Eur. Phys. J. E **26**(1–2), 217–223 (2008). https://doi.org/10.1140/epje/i2007-10315-0
50. L. Chiappisi, I. Hoffmann, M. Gradzielski, Membrane stiffening in chitosan mediated multilamellar vesicles of alkyl ether carboxylates. J. Colloid Interface Sci. **627**, 160–167 (2022)
51. W. Helfrich, Steric interaction of fluid membranes in multilayer systems. Zeitschrift für Naturforschung A **33**(3), 305–315 (1978)
52. J.B. Hayter, J. Penfold, Self-consistent structural and dynamic study of concentrated micelle solutions. J. Chem. Soc. Faraday Trans. 1 Phys. Chem. Condens. Phases **77**(8), 1851–1863 (1981)
53. M. Heinen, P. Holmqvist, A.J. Banchio, G. Nägele, Short-time diffusion of charge-stabilized colloidal particles: generic features. J. Appl. Crystallogr. **43**(5 Part 1), 970–980 (2010). https://doi.org/10.1107/S002188981002724X
54. C. Haro-Perez, M. Quesada-Pérez, J. Callejas-Fernandez, E. Casals, J. Estelrich, R. Hidalgo-Alvarez, Interplay between hydrodynamic and direct interactions using liposomes. J. Chem. Phys. **119**(1), 628–634 (2003)
55. J.F. Nagle, Introductory lecture: Basic quantities in model biomembranes. Faraday Discuss. **161**, 11–150 (2013)
56. D. Marsh, Elastic curvature constants of lipid monolayers and bilayers. Chem. Phys. Lipid. **144**(2), 146–159 (2006)
57. G. Niggemann, M. Kummrow, W. Helfrich, The bending rigidity of phosphatidylcholine bilayers: dependences on experimental method, sample cell sealing and temperature. J. Phys. II **5**(3), 413–425 (1995)
58. M. Doktorova, D. Harries, G. Khelashvili, Determination of bending rigidity and tilt modulus of lipid membranes from real-space fluctuation analysis of molecular dynamics simulations. Phys. Chem. Chem. Phys. **19**(25), 16806–16818 (2017). https://doi.org/10.1039/C7CP01921A
59. J. Henriksen, A.C. Rowat, E. Brief, Y. Hsueh, J. Thewalt, M. Zuckermann, J.H. Ipsen, Universal behavior of membranes with sterols. Biophys. J . **90**(5), 1639–1649 (2006)
60. R.M. Venable, F.L.H. Brown, R.W. Pastor, Mechanical properties of lipid bilayers from molecular dynamics simulation. Chem. Phys. Lipids **192**, 60–74 (2015). https://doi.org/10.1016/j.chemphyslip.2015.07.014
61. H. Bouvrais, L. Duelund, J.H. Ipsen, Buffers affect the bending rigidity of model lipid membranes. Langmuir **30**(1), 13–16 (2014)
62. J.R. Henriksen, J.H. Ipsen, Measurement of membrane elasticity by micro-pipette aspiration. Eur. Phys. J. E **14**(2), 149–167 (2004). https://doi.org/10.1140/epje/i2003-10146-y
63. Y. Liu, Intermediate scattering function for macromolecules in solutions probed by neutron spin echo. Phys. Rev. E **95**(2), 020501 (2017)
64. B. Brüning, R. Stehle, P. Falus, B. Farago, Influence of charge density on bilayer bending rigidity in lipid vesicles: a combined dynamic light scattering and neutron spin-echo study. Eur. Phys. J. E **36**, 1–8 (2013)
65. J.L. Cascales, S.O. Costa, A. Garro, R.D. Enriz, Mechanical properties of binary DPPC/DPPS bilayers. RSC Adv. **2**(31), 11743–11750 (2012)
66. A.-F. Bitbol, J.-B. Fournier, M.I. Angelova, N. Puff, Dynamical membrane curvature instability controlled by intermonolayer friction. J. Phys. Condens. Matter **23**(28), 284102 (2011). https://doi.org/10.1088/0953-8984/23/28/284102
67. F. Campelo, C. Arnarez, S.J. Marrink, M.M. Kozlov, Helfrich model of membrane bending: from Gibbs theory of liquid interfaces to membranes as thick anisotropic elastic layers. Adv. Colloid Interface Sci. **208**, 25–33 (2014). https://doi.org/10.1016/j.cis.2014.01.018
68. J.-H. Lee, S.-M. Choi, C. Doe, A. Faraone, P.A. Pincus, S.R. Kline, Thermal fluctuation and elasticity of lipid vesicles interacting with pore-forming peptides. Phys. Rev. Lett. **105**(3), 038101 (2010)
69. A.-F. Bitbol, D. Constantin, J.-B. Fournier, Bilayer elasticity at the nanoscale: the need for new terms. PLoS ONE **7**(11), 48306 (2012). https://doi.org/10.1371/journal.pone.0048306
70. M. Hu, D.H. Jong, S.J. Marrink, M. Deserno, Gaussian curvature elasticity determined from global shape transformations and local stress distributions: a comparative study using the martini model. Faraday Discuss. **161**, 365–382 (2013). https://doi.org/10.1039/C2FD20087B